International Journal of Nanomedicine

Dovepress
open access to scientific and medical research

Open Access Full Text Article

ORIGINAL RESEARCH

Sub-10 nm Cu_5FeS_4 cube for magnetic resonance imaging-guided photothermal therapy of cancer

This article was published in the following Dove Press journal:
International Journal of Nanomedicine

Dan Wang[1]
Yuwen Zhang[1]
Qi Guo[2]

[1]Department of Pathology, The First People's Hospital of Shangqiu, Shangqiu, Henan 476000, China; [2]Department of Orthopedics, The First People's Hospital of Shangqiu, Shangqiu, Henan 476000, China

Background: Facile synthesis and small size theranostic agents have shown great potential for cancer diagnosis and treatment.

Purpose: A ternary compound (Cu_5FeS_4), Fe doped copper sulfide, with novel magnetic properties and strong near-infrared absorption was prepared for magnetic resonance imaging (MRI) imaging guided photothermal therapy of cancer.

Patients and methods: Firstly, the capability of magnetic resonance imaging based on the novel magnetic properties and the photothermal performance due to the strong near-infrared absorption was investigated in vitro. Then, the magnetic resonance imaging guided photothermal therapy for 4T1 tumor-bearing mouse was carried out.

Results: The Cu_5FeS_4 cube with good T_1-weighted MRI, excellent photothermal performance and low cytotoxicity has been investigated. More importantly, the T_1-weighted MRI for 4T1 tumor-bearing mouse will get the best contrast effect at tumor site after 8 h of intravenous injection of Cu_5FeS_4 cube. Under the guidance of the T_1-weighted MRI, the PTT was carried out at 8 h after intravenous injection of Cu_5FeS_4 cube and only the group combined intravenous administration of Cu_5FeS_4 cube and laser irradiation nearly cured the tumor after 14 days.

Conclusion: Our study not only provides a new material for personalized treatment of tumors, but also further promotes potential applications of the cancer theranostic agents.

Keywords: magnetic nanoparticle, imaging, theranostic, 4T1, ultra-small

Introduction

During the past decade, theranostics combined imaging-based diagnosis and therapy function has received great attention because of considerable roles in tumor diagnosis and personalized treatment guidance.[1–3] Until now, several imaging technology has been developed for cancer diagnosis, including magnetic resonance imaging (MRI),[4] photoluminescence (PL) imaging,[5] photoacoustic (PA),[6] ultrasound (US) imaging,[7] X-ray computed tomography (X-ray CT) imaging,[8] and positron emission tomography (PET) imaging.[9] Compared with other imaging technologies, MRI exhibits a wide range of applications, is a nonintrusive technique, is safe (nonradiation), and has excellent high spatial resolution, which can afford evident anatomical details and soft tissue (eg, tumor) contrast.[10,11] Photothermal therapy (PTT) is a minimally invasive treatment technique, which uses the hyperthermia converted from near-infrared (NIR) laser energy to kill cancer cells. It was rapidly developed recently due to its operation simple, safety, small side effects and less pain for patient.[12,13] Therefore, the integration of MRI and PTT can result in minimal invasiveness, economic viability, and improved therapeutic efficacy.[14–17]

Nanotechnology offered numerous opportunities for integrating the MRI and PTT.[18,19] To date, a number of nanomaterials with various building blocks have been explored as an MRI-guided PTT theranostic agent for cancer.[20,21] Most of the

Correspondence: Dan Wang
Department of Pathology, The First People's Hospital of Shangqiu, Shangqiu, Henan 476000, China
Tel/fax +86 370 325 5296
Email wangdan19830101@126.com

submit your manuscript | www.dovepress.com
Dovepress
http://dx.doi.org/10.2147/IJN.S181056

MRI-guided PTT theranostic agents can be divided into two categories according to the relaxation process of the MRI agents. One is T_1 (longitudinal relaxation time)-weighted MRI-guided PTT agents based on the nanomaterials containing Gd and Mn elements. For example, Zhao and coworkers[22] developed a Gd-hybridized plasmonic Au-nanocomposite, which is based on mesoporous silica-coated AuNR with loading citrate–Gd complexes for T_1-weighted MRI-guided PTT for cancer. Another type is T_2 (transverse relaxation time)-weighted MRI-guided PTT agents based on the nanomaterials containing Fe element. NIR light-absorbing polymer-coated iron oxide nanoclusters were developed by Liu et al,[23] and the composites possess highly effective photothermal treatment recorded by T_2-weighted MRI. Compared with the T_2-weighted MRI, T_1-weighted MRI has obvious advantage on soft tissue contrast due to the positive signal.[10] However, the potential toxicity of Gd limited the application of the T_1-weighted MRI agents.[24] In addition, the multistep prepared method or big size for most of the obtained MRI-guided PTT theranostic agents also limited the wide application for cancer diagnosis and treatment.[25–27] Thus, it is very significant to develop the new T_1-weighted MRI-guided PTT agents with facile synthesis and small size.

Several kinds of PTT agents have been developed including noble metal structure,[28] organic dyes and polymer,[29] carbon-based materials,[30] and inorganic compound.[31,32] Particularly, inorganic compound including metal sulfide and metal oxide was investigated widely as the PTT agents because of their easy preparation and low cost. CuS is one of the popular inorganic compound PTT agents due to the strong NIR localized surface plasmon resonance (LSPR) absorption and low toxicity.[33–35] In addition, there are many kinds of ternary composites based on copper sulfide (eg, Cu_5FeS_4), and the preparation method is also simple.[36–38] Therefore, it is facile to design and synthesize T_1-weighted MRI-guided PTT agents based on ternary composites of copper sulfide.[39–41] Herein, a Cu_5FeS_4 cube with a diameter of ~5 nm was prepared by a simple one-pot pyrolysis of the mixture of iron acetylacetonate and copper acetylacetonate. Then, the T_1-weighted MRI-guided PTT for cancer based on this small Cu_5FeS_4 cube was investigated.

Materials and methods

Chemicals

All chemicals and reagents were used as purchased without further purification. Iron acetylacetonate, copper acetylacetonate, and 1-dodecanethiol were purchased from Aladdin Reagent Co. Ltd. (Shanghai, China). 1,2-Distearoyl-sn-glycero-3-phosphoethanol-amine-*N*-[methoxy(polyethyleneglyco)-2000] (DSPE-PEG2000) was purchased from Nanocs Inc. (New York, NY, USA).

Characterization

TEM was performed using a transmission electron microscope (JEOL JEM-2100 at 200 kV). X-ray diffraction (XRD) was carried out on a Rigaku D/MAX 2250 diffractometer with Cu/Kα radiation at a scanning rate of 10°/min in the 2θ range of 20–80°. The hysteresis loop was detected by a magnetometer (SQUID; Quantum Design, Inc., San Diego, CA, USA). Ultraviolet-visible (UV-vis) absorption spectra were acquired on a UV-2550 UV-Vis-NIR spectrophotometer (Shimadzu, Kyoto, Japan). Magnetic resonance relaxometry was conducted on a NMI20 Analyst (Niumag, Shanghai, China). The Fe content in the samples was tested by inductively coupled plasma atomic emission spectroscopy (ICP-AES).

Synthesis of Cu_5FeS_4 cube

Cu_5FeS_4 cube was synthesized by one-pot pyrolysis method. 0.5 mmol copper acetylacetonate and 0.1 mmol iron acetylacetonate were dissolved in 20 mL 1-dodecanethiol at room temperature. Then, the mixture was heated at 120°C for 1 hour to remove the dissolved oxygen and water. After that, the temperature was increased to 200°C at the rate of 10°C/min and kept for 20 minutes. Finally, the Cu_5FeS_4 cube was precipitated by ethanol and collected by centrifugation.

DSPE-PEG2000-modified Cu_5FeS_4 cube

According to the previous study,[42] 1-dodecanethiol-coated Cu_5FeS_4 cube in chloroform (0.5 mL, 10 mg/mL) was added to DSPE-PEG2000 (10 mg in 2 mL of chloroform) in a glass vial and shaken for overnight. After removing the solvent completely, 5 mL of water was added. Finally, the DSPE-PEG2000-modified Cu_5FeS_4 cube was obtained by removing the excess DSPE-PEG2000 using dialysis (molecular weight cutoff [MWCO], 14,000) and filtering using the 0.1 μm cellulose acetate syringe filter.

Photothermal performance tests

To detect the photothermal performance of the obtained Cu_5FeS_4 cube, the FLIR A300 thermal camera (FLIR® Systems, Inc., New York, NY, USA) was used to record the temperature changes of water and Cu_5FeS_4 cube water dispersion (25, 50, 75, and 100 μg/mL) under the irradiation of 808 nm laser (1 W/cm^2) for 15 minutes. For the photostability tests, the heat generation of 80 μg/mL Cu_5FeS_4 cube water dispersion was tested for eight cycles of laser irradiation (15 minutes on and 15 minutes off).

In vivo MRI studies

The in vivo MR images were carried out on a 4T1 tumor-bearing mouse model by 0.5 T MRI system (MiniMR-60; Niumag). The 4T1 tumor-bearing mouse was constructed by injecting 4T1 cells into the right hind legs of BALB/c nude mice (Shanghai Laboratory Animal Center). The MR images were collected before (0 hour) and after (4, 8, and 24 hours) injection of Cu_5FeS_4 cube via tail vein with a dosage of 1.8 mg/kg. Mice selection, methods of care, and sacrificing were approved by the Animal Ethics Committee of The First People's Hospital of Shangqiu and strictly conducted in accordance with the policy of the Institutional Animal Care and Use Committee.

In vitro biocompatibility

The biocompatibility of Cu_5FeS_4 cube was quantitatively investigated by the Cell Counting Kit-8 (CCK-8) assay. First, the breast cancer cells (4T1; Shanghai Institutes for Biological Sciences, Shanghai, China) and human umbilical vein endothelial cells (HUVECs; Shanghai Institutes for Biological Sciences) were incubated with 100 μL PBS and 100 μL Cu_5FeS_4 cube PBS dispersion with different concentrations (10, 25, 50, 100, and 200 μg/mL) for 12 and 24 hours, respectively. Then, 10 μL CCK-8 was added and incubated for 30 minutes at 37°C. After that, the absorbance at 450 nm was recorded using a microplate reader (Varioskan Flash; Thermo Fisher Scientific, Waltham, MA, USA).

In vivo PTT therapy

After the tumor volume was grown to ~100 mm^3, the 4T1 tumor-bearing mice were randomly assigned to four groups: 1) PBS alone; 2) PBS+laser; 3) Cu_5FeS_4 cube alone; 4) Cu_5FeS_4 cube+laser. 200 μL PBS was injected to the mice of groups 1 and 2, while the Cu_5FeS_4 cube was injected to groups 3 and 4 via the tail vein with a dosage of 1.8 mg/kg. After 8 hours of the injection, the mice in groups 2 and 4 were irradiated by 808 nm laser (1 W/cm^2) for 5 minutes, and the NIR thermal images of the mice of these two groups also were recorded. Following, the tumor volumes and weight of the mice were monitored daily for up to 14 days.

Results and discussion

Synthesis and characterization of Cu_5FeS_4 cube

Simple pot pyrolysis method was used to synthesize Cu_5FeS_4 cube. Briefly, the mixture of copper acetylacetonate, iron acetylacetonate, and 1-dodecanethiol was heated at 200°C for 20 minutes. Then, the Cu_5FeS_4 cube was formed by the combination of Cu in copper acetylacetonate, the Fe in Iron acetylacetonate, and S in 1-dodecanethiol after the reaction. Finally, the prepared sample was purified by the centrifugation. The crystalline structures and phase composition of the obtained sample nanoparticles were determined by XRD. As shown in Figure 1A, the diffraction peaks at 28.1, 32.5, 46.7, and 55.4° (2θ) of the obtained sample are well indexed to the (111, 200, 220) and (311) plane of cubic bornite Cu_5FeS_4 crystal (Joint Committee on Powder Diffraction Standards card no. 24–0050). The broad diffraction peak was assigned to small size of the prepared Cu_5FeS_4 crystal. The morphology and size of the obtained Cu_5FeS_4 crystal were observed by the TEM. As shown in Figure 1B, the obtained Cu_5FeS_4 crystal has a uniform cube morphology with a mean diameter of 5±1 nm. The observed clear (lattice plane 200 with d-spacing of ~0.27 nm) lattice fringes of cubic bornite Cu_5FeS_4 crystal by the HR-TEM image further confirm the high crystallinity of the obtained Cu_5FeS_4 cube (Figure 1C). The aforementioned results suggest that the Cu_5FeS_4 cube with ultra-small size has been prepared successfully.

To demonstrate if the Cu_5FeS_4 cube has similar NIR absorption with the copper sulfide, the UV-vis-NIR spectra were used to record the absorption of the Cu_5FeS_4 cube. As shown in Figure 2A, the UV-vis-NIR spectra show an intense broad band extending in the entire NIR region (700–1,000), which is assigned to LSPR of the prepared Cu_5FeS_4 cube similar to the copper sulfide. Compared with the copper sulfide, the doped Fe ion will not affect the LSPR absorption in the NIR region. More importantly, the strong absorption in the NIR region is beneficial for the photothermal conversion according to the previous study.[33] Thus, the Cu_5FeS_4 cube, a ternary compound based on the copper sulfide, shows a great potential as the PTT agents. To evaluate that the introduction of Fe ions in the ternary compound based on copper sulfide will generate the interesting magnetic properties as our design, the hysteresis loop which has the plots of magnetization vs magnetic field (M-H loop) was carried out at room temperature. As shown in Figure 2B, the hysteresis loop suggests that the magnetization value is 0.966 emu/g, and no coercivity was observed, indicating the superparamagnetic nature of the prepared Cu_5FeS_4 cube. The superparamagnetic nature of Cu_5FeS_4 cube can be used for MRI. The strong NIR absorption and superparamagnetic nature of the Cu_5FeS_4 cube indicate the potential for MRI-guided PTT for cancer.

Photothermal and magnetic properties

The prerequisite of the MRI contrast and PTT agent is that the Cu_5FeS_4 cube must be dispersed in water very well. Thus, DSPE-PEG2000 was used to modify the Cu_5FeS_4 cube according to the previous method.[42] The amphiphilic

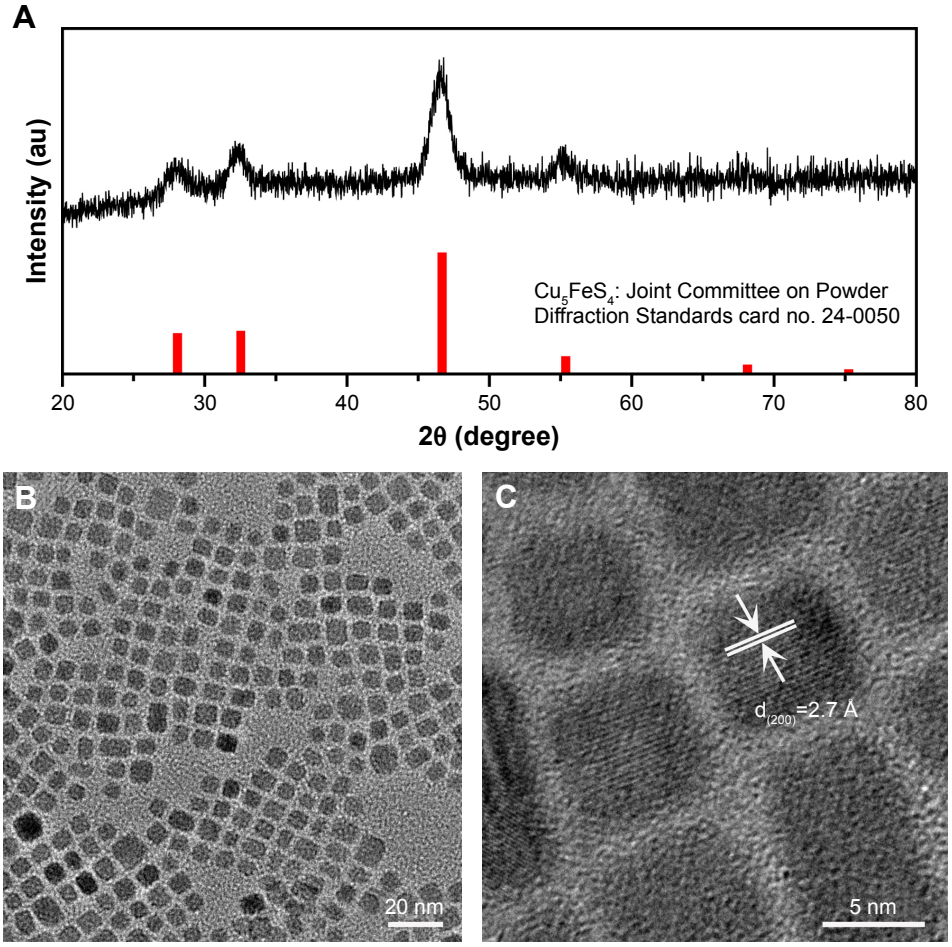

Figure 1 (**A**) XRD, (**B**) TEM, and (**C**) HR-TEM characterization of the obtained Cu_5FeS_4 cube nanoparticles.
Abbreviation: XRD, X-ray diffraction.

DSPE-PEG2000 can transform the hydrophobic nanoparticles to hydrophilic nanoparticles through the hydrophobic effect (Figure 3A). The dispersion stability of the nanocrystals in water was evaluated by the absorbance at 808 nm of the Cu_5FeS_4 cube dispersed in water after modification with time going. As shown in Figure 3B, the absorbance at 808 nm in the Cu_5FeS_4 cube shows no obvious change after 7 days, indicating the good stability in water. Then, the photothermal

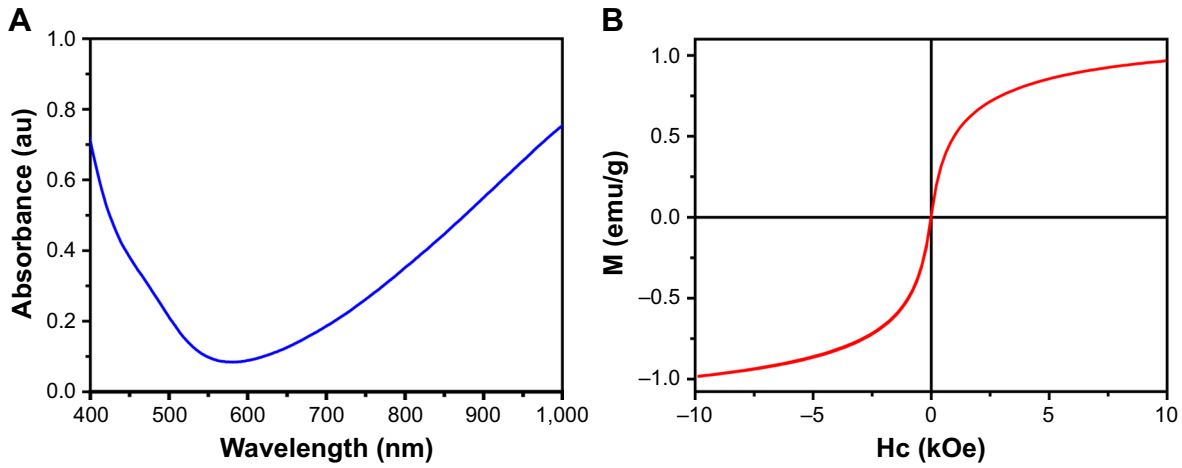

Figure 2 (**A**) UV-vis-NIR spectrum and (**B**) hysteresis loop of the obtained Cu_5FeS_4 cube nanoparticles.
Abbreviations: Hc, coercive force Hc; M, magnetization; NIR, near-infrared; UV-vis, ultraviolet-visible.

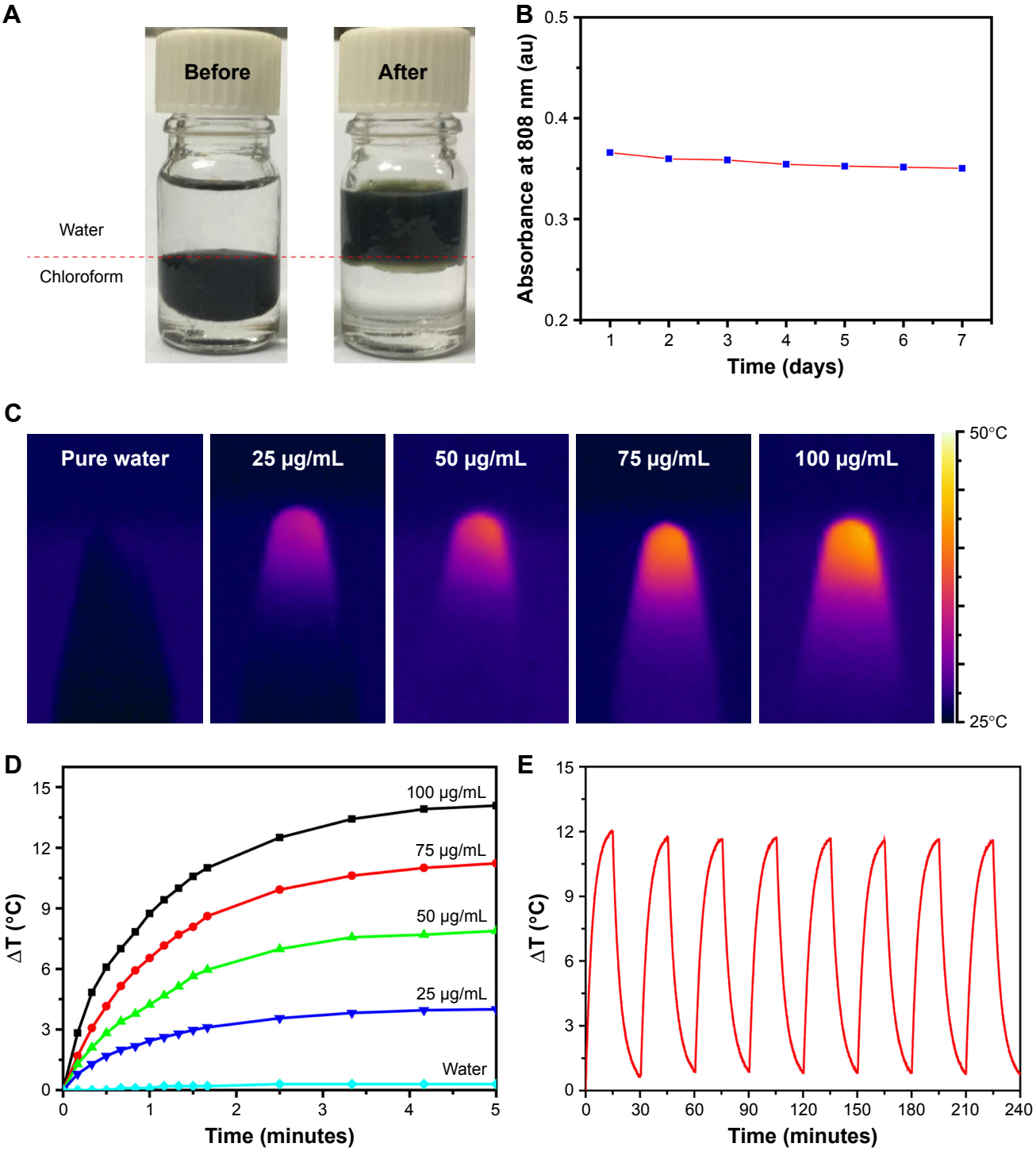

Figure 3 (**A**) Photograph of the Cu_5FeS_4 dispersed in chloroform and water before and after surface modification. (**B**) The absorbance intensity at 808 nm curve with time for the Cu_5FeS_4 dispersed in water. (**C**) NIR photothermal images and (**D**) corresponding heating curves of pure water and Cu_5FeS_4 cube nanoparticles aqueous dispersions with different concentrations under 808 nm laser irradiation (1 W/cm^2) for 5 minutes. (**E**) Photothermal performance for Cu_5FeS_4 cube nanoparticles aqueous dispersions after eight cycles of laser on/off.
Abbreviation: NIR, near-infrared.

performance of the obtained DSPE-PEG2000-modified Cu_5FeS_4 cube was investigated. The hydrophilic Cu_5FeS_4 cube was dispersed in water at different concentrations from 25 to 100 μg/mL. The temperature change of pure water and Cu_5FeS_4 cube water dispersion was recorded by the FLIR A300 thermal camera under the laser irradiation for 5 minutes with a power density of 1 W/cm^2. As shown in Figure 3C, the color of the thermal images of pure water changed little, while the color changed greatly with the increase in concentration for the Cu_5FeS_4 cube. The heating curves shown in Figure 3D

and E exhibit the similar trend, the temperature of the Cu_5FeS_4 cube (100 μg/mL) increases by 14.75°C and water only by 0.4°C. These results demonstrate that Cu_5FeS_4 cube shows excellent photothermal conversion performance. Photostability is also important for the PTT agents. The photothermal performance of the Cu_5FeS_4 cube after eight cycles of laser on/off was used to evaluate the photostability. As shown in Figure 3E, the temperature can be increased to nearly same degree from the initial temperature after eight cycles of laser on/off (15 minutes on and 15 minutes off), indicating the good photostability of the Cu_5FeS_4 cube. The excellent photothermal conversion performance and good photostability suggest that the Cu_5FeSe_4 cube is an ideal PTT agent.

Encouraged by the superparamagnetic nature of the Cu_5FeS_4 cube due to the doped Fe ion, we next studied the longitudinal relaxivity and T_1-weighted MRI contrast performance in water by the NMI20 Analyst. First, the Fe content of each sample was detected by ICP-AES analysis and the longitudinal relaxation time was recorded by the NMI20 Analyst. Then, the relaxivity was calculated by the plots of $1/T_1$ vs Fe concentration. As shown in Figure 4A, the value of longitudinal relaxivity (r_1) is 0.43 mM/s, which is smaller than the 0.9138 mM/s of 20 nm Cu_5FeS_4 but bigger than the 0.20 mM/s of ultra-small $CuFeSe_2$ (~0.41 nm). The T_1-weighted MRI in water also was conducted on the NMI20 Analyst. Figure 4B shows that the T_1-weighted MRI image is very dark the absence of Cu_5FeS_4 cube (water only), while the T_1-weighted MRI images in the presence of Cu_5FeS_4 cube change brighter and brighter with the increase of Fe concentration from 0.027 to 0.207 mM. The good contrast performance at very low Fe concentration (0.207 mM) suggests that the Cu_5FeS_4 cube is a good T_1-weighted MRI agent.

Biocompatibility

The biocompatibility to the materials is very important for bioapplication, especially when used in vivo. To assess the cytotoxicity of the prepared Cu_5FeS_4 cube, the CCK-8 assay was used to test the cell viability after incubation with the Cu_5FeS_4 cube for 12 and 24 hours. Here, to make the test result more representative, two different kinds of cells were chosen, one is a normal HUVECs and the other is a breast cancer cell lines (4T1). As shown in Figure 5A and B, the viability for HUVEC is >80% after incubation with the Cu_5FeS_4 cube for both 12 and 24 hours when the concentration is <200 mM, while the 4T1 is >90%. These results show that the cytotoxicity of the prepared Cu_5FeS_4 cube is very low and is beneficial for further bioapplication in vivo, which is similar to the previous results of copper sulfide.[35]

In vivo MRI

The low cytotoxicity, good T_1-weighted MRI effect, and excellent photothermal performance of the prepared Cu_5FeS_4 cube have driven us to explore the T_1-weighted MRI-guided PTT for cancer in vivo. The 4T1 tumor-bearing mouse was used as the tumor model, and the mouse without injection of the Cu_5FeS_4 cube was used as a control. Once the mouse was intravenously injected with the Cu_5FeS_4 cube, the T_1-weighted MR image was collected at 4, 8, and 24 hours on MRI system. As shown in Figure 6A, the tumor site (marked with red ellipse) was not very clear without the intravenous injection of the Cu_5FeS_4 cube (0 hour). After 4 hours of the intravenous injection of the Cu_5FeS_4 cube, the tumor site appeared brighter and increased to brightest at 8 hours, which means more and more injected Cu_5FeS_4 cubes were accumulated at the tumor site due to the enhanced permeability and

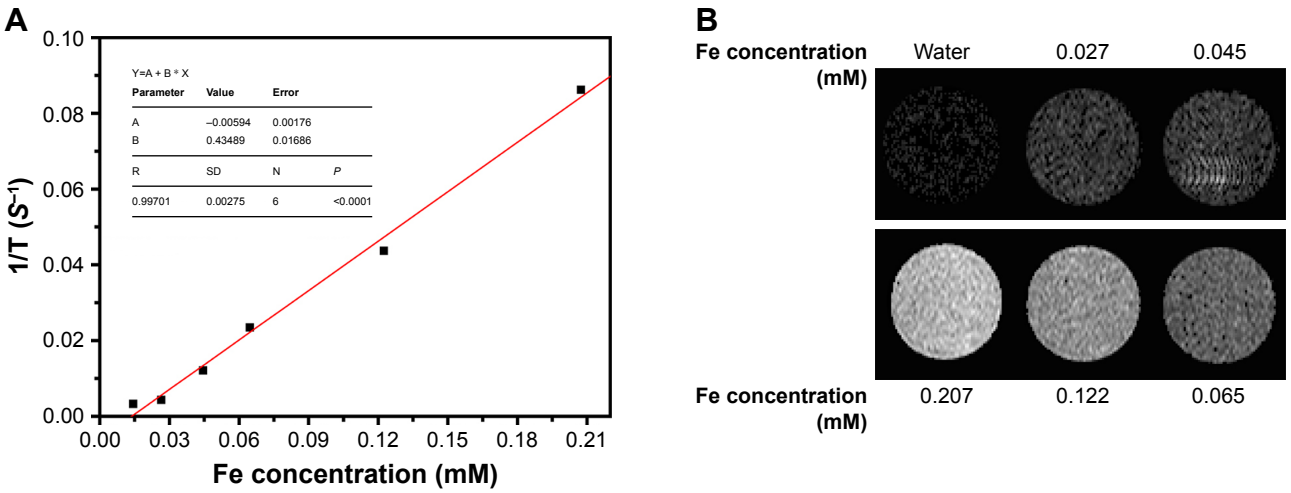

Figure 4 (**A**) Plots of $1/T_1$ vs Fe concentration and (**B**) T_1-weighted MR images of Cu_5FeS_4 cube nanoparticles aqueous dispersions with concentrations ranging from 0 to 0.207 mM.

Abbreviations: MR, magnetic resonance; T_1, longitudinal relaxation time.

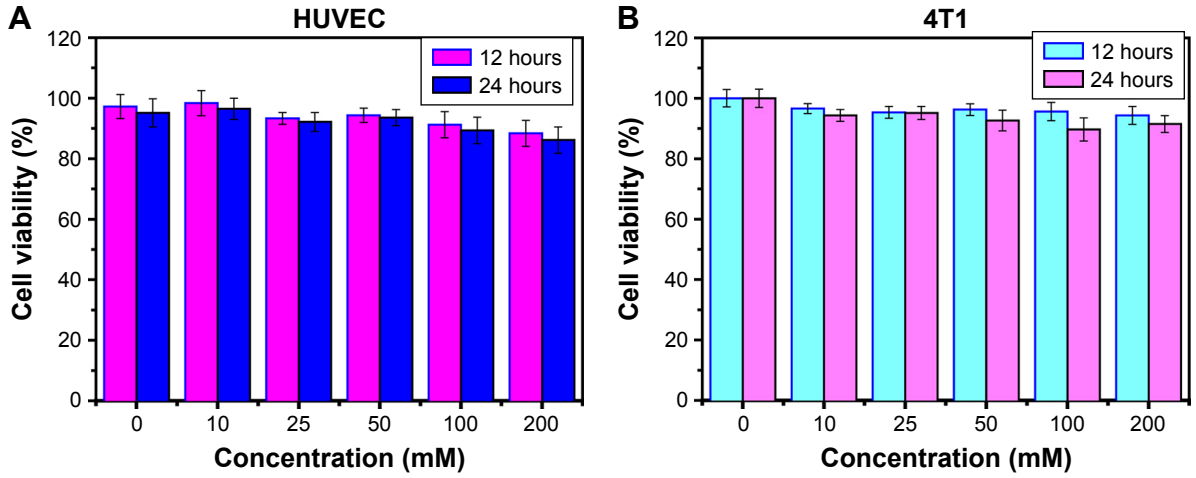

Figure 5 In vitro viabilities of HUVEC (**A**) and 4T1 cells (**B**) after incubation with various concentrations of Cu_5FeS_4 cube nanoparticles for 12 and 24 hours, respectively.
Abbreviation: HUVEC, human umbilical vein endothelial cell.

retention (EPR) effect. The MR image nearly decreased to control after 24 hours of injection, which can be assigned to remove the Cu_5FeS_4 cube from the tumor site. The MRI images (Figure 6A) corresponded signal value (Figure 6B) also present similar trend that the value increased with time going on from 0 to 8 h and then decreased nearly to control (0 h) at 24 h. The obvious contrast change on the MR images for tumor site with time going on suggest that the prepared Cu_5FeS_4 cube can be used for cancer diagnosis. Due to the positive correlation between the brightness of the MR images and the concentration of the contrast agent, an MRI can be used to measure the accumulated dosage of the injected Cu_5FeS_4 cube in real time at the tumor site. Therefore, the optimal treatment time for PTT can also be guided by the MRI, which means that it will get the best PTT treatment effect if the tumor is irradiated by laser at 8 hours in our case according to the MRI results.

In vivo PTT

The 4T1 tumor-bearing mouse was used as the tumor model to evaluate the PTT effect. The 4T1 tumor-bearing mouse was randomly divided into four groups: PBS, PBS+laser, Cu_5FeS_4, and Cu_5FeS_4+laser. The PBS group treated with only intravenous injection of PBS was used as the control group; the PBS+laser group treated by both intravenous injection of PBS and laser irradiation was used to evaluate

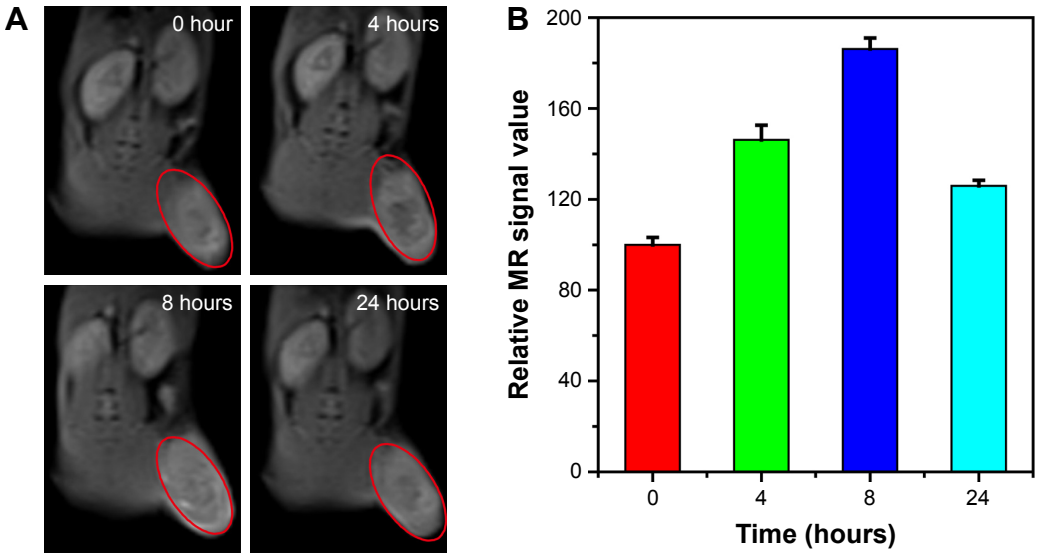

Figure 6 (**A**) Time-dependent in vivo MR imaging and (**B**) corresponding MR signal intensities in 4T1 tumor-bearing mice before (0 hour) and after (4–24 hours) intravenous injection of Cu_5FeS_4 cube nanoparticles.
Abbreviation: MR, magnetic resonance.

the PTT effect based on the laser; the Cu_5FeS_4 group injected only with the Cu_5FeS_4 cube via the tail vein was used to assess the PTT effect of the Cu_5FeS_4 cube; and the Cu_5FeS_4+laser group treated with laser irradiation after the intravenous injection of the Cu_5FeS_4 cube was used to investigate the PTT effect based on Cu_5FeS_4 with laser irradiation. Based on the guidance of the MRI, the PTT was carried out at 8 hours after intravenous injection of the Cu_5FeS_4 cube. Because the temperature at the tumor site will be changed only under the laser irradiation, the mice for PBS+laser and Cu_5FeS_4+laser groups were monitored by the thermal camera (FLIR A300 thermal camera) throughout the PTT process. As shown in Figure 7A, the initial temperature (0 h) of the mice for both of the two groups is similar where the color of the thermal images are nearly same. After irradiation by laser for 5 minutes, the color of the thermal images of Cu_5FeS_4+laser group changed more obviously compared with the PBS+laser group. The corresponding curves of temperature change in the two groups also demonstrate that the temperature of the Cu_5FeS_4+laser group will increase from 33°C to 49°C and temperature of the PBS+laser group only increase from 33°C to 41.5°C (Figure 7B). The great temperature change in tumor site of mouse for the Cu_5FeS_4+laser group is attributed to the good photothermal performance of Cu_5FeS_4 cube and the higher accumulated dosage at 8 hours after intravenous injection of the Cu_5FeS_4 cube. More importantly, the tumor will be destroyed by the temperature of 49°C obtained by the Cu_5FeS_4 cube under the laser irradiation.

Thereafter, the PTT in different groups, the size of tumor, body weight, drinking, and eating were observed in all experimental groups within 2 weeks of treatment, and the size of the tumor was tested daily and weight was recorded every 2 days. During monitoring time, all the mice exhibit no obvious sign of toxic side effects or abnormal neurological issues including activity, drinking, and eating. Figure 8A shows the mice of the four groups treated with different methods at 0 and 14 days and Figure 8B shows the tumor size vs the time after different treatments. For the mice of PBS group, the tumor necrosis was obtained at 14 days (Figure 8A, left-most) and the tumor size (Figure 8B, black line) increased quickly with increase in time as PBS cannot inhibit the excessive growth of tumor. Similarly, the tumor necrosis was obtained at 14 days for both the PBS+laser group and Cu_5FeS_4 group (Figure 8A, left-center and right-center, respectively). Compared with the PBS alone group, the growth of the tumor size in both PBS+laser group and Cu_5FeS_4 group is little slow (Figure 8B, red and green line, respectively), indicating that the laser or Cu_5FeS_4 alone has only a minimal effect on the excessive growth of tumor. Encouragingly, the tumor nearly disappeared at 14 days (Figure 8A, right-most) and the tumor size decreased quickly (Figure 8B blue line) for the Cu_5FeS_4+ laser group, which was treated by the laser irradiation after intravenous injection of the Cu_5FeS_4 cube at 8 hours. The disappeared tumor can be attributed that the tumor was destroyed by the high temperature generated by the accumulated Cu_5FeS_4 cubes in the tumor under the laser irradiation. As shown in Figure 8C, there is no significant change in body weight during treatment, which means that the toxicity of material in mice is very low. These results suggest that the Cu_5FeS_4 cube can cure the tumor effectively combining intravenous administration of Cu_5FeS_4 cube and laser irradiation.

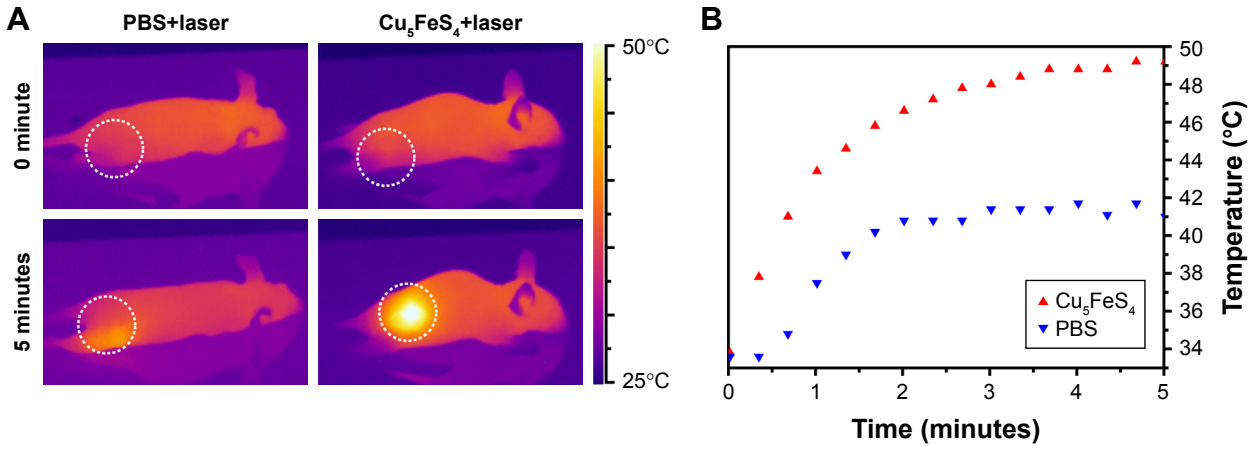

Figure 7 (**A**) In vivo NIR photothermal imaging and (**B**) corresponding curves of temperature change of 4T1 tumor-bearing mice before and after intravenous injection with PBS or Cu_5FeS_4 cube nanoparticles followed by a 808 nm laser (1 W/cm^2) irradiation for 5 minutes.
Abbreviation: NIR, near-infrared.

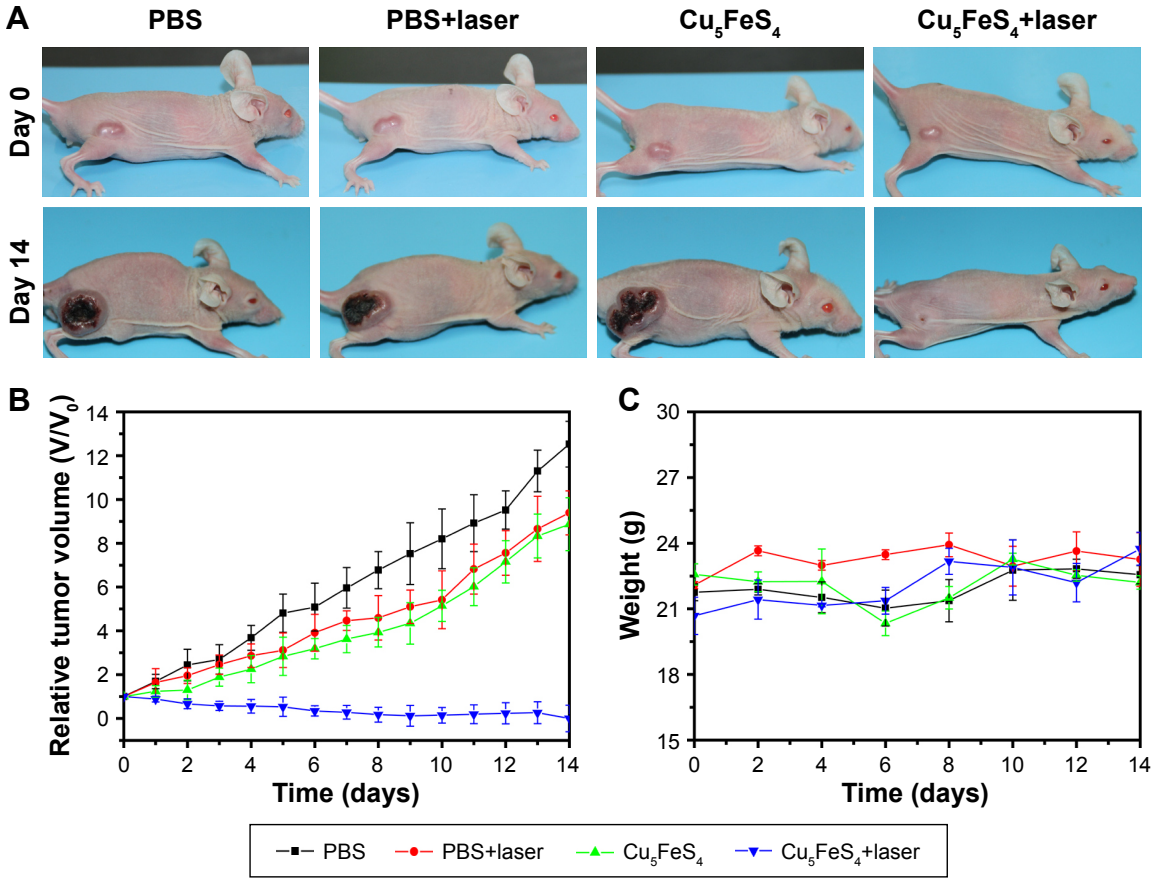

Figure 8 (**A**) Representative photograph of the mice bearing tumors before (0 day) and after 14 days treatment; (**B**) profiles of the tumor volumes on the mice with different treatment groups (PBS only, PBS+laser, Cu_5FeS_4 only, and Cu_5FeS_4+laser) from 0 to 14 days; (**C**) the weight of mice bearing tumors recorded every day from 0 to 14 days after treatment for different treatment groups (PBS only, PBS+laser, Cu_5FeS_4 only, and Cu_5FeS_4+laser).

Conclusion

A ternary compound (Cu_5FeS_4 cube) with a mean diameter of 5±1 nm based on a facile one-pot pyrolysis method has been prepared successfully. The obtained Cu_5FeS_4 cube not only possesses strong NIR absorption like copper sulfide but also exhibits novel magnetic properties due to the doped Fe ion. Furthermore, the Cu_5FeS_4 cube with good T_1-weighted MRI, excellent photothermal performance, and low cytotoxicity has been investigated. More importantly, the T_1-weighted MRI for 4T1 tumor-bearing mouse will get the best contrast effect at the tumor site after 8 hours of intravenous injection of the Cu_5FeS_4 cube. Under the guidance of the T_1-weighted MRI, the PTT was carried out at 8 hours after intravenous injection of the Cu_5FeS_4 cube and only the group combined intravenous administration of Cu_5FeS_4 cube and laser irradiation nearly cured the tumor after 14 days. Our study not only provides a new material for personalized treatment of tumors but also further promotes potential applications of the cancer theranostic agents.

Acknowledgment

This work was partially supported by The First People's Hospital of Shangqiu.

Disclosure

The authors report no conflicts of interest in this work.

References

1. Chen Q, Liang C, Sun X, et al. H_2O_2-responsive liposomal nanoprobe for photoacoustic inflammation imaging and tumor theranostics via in vivo chromogenic assay. *Proc Natl Acad Sci U S A*. 2017;114(21):5343–5348.
2. Wen J, Yang K, Liu F, Li H, Xu Y, Sun S. Diverse gatekeepers for mesoporous silica nanoparticle based drug delivery systems. *Chem Soc Rev*. 2017;46(19):6024–6045.
3. Mu X, Yan C, Tian Q, Lin J, Yang S. BSA-assisted synthesis of ultrasmall gallic acid-Fe(III) coordination polymer nanoparticles for cancer theranostics. *Int J Nanomedicine*. 2017;12:7207–7223.
4. Mitsouras D, Lee TC, Liacouras P, et al. Three-dimensional printing of MRI-visible phantoms and MR image-guided therapy simulation. *Magn Reson Med*. 2017;77(2):613–622.
5. Wang H, Mukherjee S, Yi J, Banerjee P, Chen Q, Zhou S. Biocompatible chitosan-carbon dot hybrid nanogels for NIR-imaging-guided synergistic photothermal-chemo therapy. *ACS Appl Mater Interfaces*. 2017;9(22):18639–18649.

6. Kim T, Zhang Q, Li J, Zhang L, Jokerst JV. A gold/silver hybrid nanoparticle for treatment and photoacoustic imaging of bacterial infection. *ACS Nano*. 2018;12(6):5615–5625.
7. Devulapally R, Lee T, Barghava-Shah A, et al. Ultrasound-guided delivery of thymidine kinase-nitroreductase dual therapeutic genes by PEGylated-PLGA/PIE nanoparticles for enhanced triple negative breast cancer therapy. *Nanomedicine*. 2018;13(9):1051–1066.
8. Shanavas A, Rengan AK, Chauhan D, et al. Glycol chitosan assisted in situ reduction of gold on polymeric template for anti-cancer theranostics. *Int J Biol Macromol*. 2018;110:392–398.
9. Sheikh-Bahaei N, Sajjadi SA, Manavaki R, et al. Positron emission tomography-guided magnetic resonance spectroscopy in Alzheimer disease. *Ann Neurol*. 2018;83(4):771–778.
10. Schuchmann S, Weigel C, Albrecht L, et al. Non-invasive quantification of hepatic fat fraction by fast 1.0, 1.5 and 3.0 T MR imaging. *Eur J Radiol*. 2007;62(3):416–422.
11. Aisen AM, Martel W, Braunstein EM, Mcmillin KI, Phillips WA, Kling TF. MRI and CT evaluation of primary bone and soft-tissue tumors. *AJR Am J Roentgenol*. 1986;146(4):749–756.
12. Cheng L, Wang C, Feng L, Yang K, Liu Z. Functional nanomaterials for phototherapies of cancer. *Chem Rev*. 2014;114(21):10869–10939.
13. Tian Q, Hu J, Zhu Y, et al. Sub-10 nm Fe3O4@$Cu_{(2-x)}$S core-shell nanoparticles for dual-modal imaging and photothermal therapy. *J Am Chem Soc*. 2013;135(23):8571–8577.
14. Wang S, Ren W, Wang J, et al. Black TiO_2-based nanoprobes for T_1-weighted MRI-guided photothermal therapy in CD133 high expressed pancreatic cancer stem-like cells. *Biomater Sci*. 2018;6(8):2209–2218.
15. Yang K, Yang G, Chen L, et al. FeS nanoplates as a multifunctional nano-theranostic for magnetic resonance imaging guided photothermal therapy. *Biomaterials*. 2015;38:1–9.
16. Yang Y, Liu J, Liang C, et al. Nanoscale Metal-Organic Particles with Rapid Clearance for Magnetic Resonance Imaging-Guided Photothermal Therapy. *ACS Nano*. 2016;10(2):2774–2781.
17. Zhang C, Wu D, Lu L, et al. Multifunctional hybrid liposome as a theranostic platform for magnetic resonance imaging guided photothermal therapy. *ACS Biomater Sci Eng*. 2018;4(7):2597–2605.
18. Xiang Y, Li N, Guo L, et al. Biocompatible and pH-sensitive MnO-loaded carbonaceous nanospheres (MnO@CNSs): A theranostic agent for magnetic resonance imaging-guided photothermal therapy. *Carbon N Y*. 2018;136:113–124.
19. Yang Z, He W, Zheng H, et al. One-pot synthesis of albumin-gadolinium stabilized polypyrrole nanotheranostic agent for magnetic resonance imaging guided photothermal therapy. *Biomaterials*. 2018;161:1–10.
20. Chen Q, Wen J, Li H, et al. Recent advances in different modal imaging-guided photothermal therapy. *Biomaterials*. 2016;106:144–166.
21. Guo H, Sun H, Zhu H, et al. Synthesis of Gd-functionalized $Fe3O_4$@polydopamine nanocomposites for T_1/T_2 dual-modal magnetic resonance imaging-guided photothermal therapy. *New J Chem*. 2018;42(9):7119–7124.
22. Wang J, Liu J, Liu Y, et al. Gd-hybridized plasmonic au-nanocomposites enhanced tumor-interior drug permeability in multimodal imaging-guided therapy. *Adv Mater*. 2016;28(40):8950–8958.
23. Wang C, Xu H, Liang C, et al. Iron oxide@polypyrrole nanoparticles as a multifunctional drug carrier for remotely controlled cancer therapy with synergistic antitumor effect. *ACS Nano*. 2013;7(8):6782–6795.
24. Pasquini L, Napolitano A, Visconti E, et al. Gadolinium-based contrast agent-related toxicities. *CNS Drugs*. 2018;32(3):229–240.
25. Ju Y, Zhang H, Yu J, et al. Monodisperse Au-Fe_2C Janus Nanoparticles: An Attractive Multifunctional Material for Triple-Modal Imaging-Guided Tumor Photothermal Therapy. *ACS Nano*. 2017;11(9):9239–9248.
26. Ji X, Kong N, Wang J, et al. A novel top-down synthesis of ultrathin 2d boron nanosheets for multimodal imaging-guided cancer therapy. *Adv Mater*. Epub 2018 Jul 18.
27. Liu Y, Yang Z, Huang X, et al. Glutathione-responsive self-assembled magnetic gold nanowreath for enhanced tumor imaging and imaging-guided photothermal therapy. *ACS Nano*. 2018;12(8):8129–8137.
28. Abadeer NS, Murphy CJ. Recent progress in cancer thermal therapy using gold nanoparticles. *J Phys Chem C*. 2016;120(9):4691–4716.
29. Song X, Chen Q, Liu Z. Recent advances in the development of organic photothermal nano-agents. *Nano Res*. 2015;8(2):340–354.
30. Chen YW, Su YL, Hu SH, Chen SY. Functionalized graphene nanocomposites for enhancing photothermal therapy in tumor treatment. *Adv Drug Deliv Rev*. 2016;105(Pt B):190–204.
31. Huang K, Li Z, Lin J, Han G, Huang P. Two-dimensional transition metal carbides and nitrides (MXenes) for biomedical applications. *Chem Soc Rev*. 2018;47(14):5109–5124.
32. Huang X, Zhang W, Guan G, Song G, Zou R, Hu J. Design and functionalization of the NIR-responsive photothermal semiconductor nanomaterials for cancer theranostics. *Acc Chem Res*. 2017;50(10):2529–2538.
33. Tian Q, Jiang F, Zou R, et al. Hydrophilic $Cu9S_5$ nanocrystals: a photothermal agent with a 2_5.7% heat conversion efficiency for photothermal ablation of cancer cells *in vivo*. *ACS Nano*. 2011;5(12):9761–9771.
34. Wang S, Riedinger A, Li H, et al. Plasmonic copper sulfide nanocrystals exhibiting near-infrared photothermal and photodynamic therapeutic effects. *ACS Nano*. 2015;9(2):1788–1800.
35. Guo L, Panderi I, Yan DD, et al. A comparative study of hollow copper sulfide nanoparticles and hollow gold nanospheres on degradability and toxicity. *ACS Nano*. 2013;7(10):8780–8793.
36. Zhao Y, Tong L, Li Z, et al. Stable and multifunctional dye-modified black phosphorus nanosheets for near-infrared imaging-guided photothermal therapy. *Chem Mater*. 2017;29(17):7131–7139.
37. Zhang BQ, Liu Y, Zuo Y, et al. Colloidal synthesis and thermoelectric properties of $CuFeSe_2$ nanocrystals. *Nanomaterials*. 2018;8(1):8.
38. Li Y, Wang Y, Pattengale B, et al. High-index faceted $CuFeS_2$ nanosheets with enhanced behavior for boosting hydrogen evolution reaction. *Nanoscale*. 2017;9(26):9230–9237.
39. Ding B, Yu C, Li C, et al. cis-Platinum pro-drug-attached $CuFeS_2$ nanoplates for in vivo photothermal/photoacoustic imaging and chemotherapy/photothermal therapy of cancer. *Nanoscale*. 2017;9(43):16937–16949.
40. Jiang X, Zhang S, Ren F, et al. Ultrasmall Magnetic $CuFeSe_2$ Ternary Nanocrystals for Multimodal Imaging Guided Photothermal Therapy of Cancer. *ACS Nano*. 2017;11(6):5633–5645.
41. Zhao Q, Yi X, Li M, et al. High near-infrared absorbing Cu_5FeS_4 nanoparticles for dual-modal imaging and photothermal therapy. *Nanoscale*. 2016;8(27):13368–13376.
42. Zhou P, Zhao H, Wang Q, et al. Photoacoustic-Enabled Self-Guidance in Magnetic-Hyperthermia Fe@Fe_3O_4 Nanoparticles for Theranostics In Vivo. *Adv Healthc Mater*. 2018;7(9):1701201.